Field-induced electronic phase separation in the high-temperature superconductor $La_{1.94}Sr_{0.06}CuO_{4+y}$

S. Holm-Dahlin,[1,*] J. Larsen,[2,3] H. Jacobsen,[1,4,5] A. T. Rømer,[1,3,6] A.-E. Ţuţueanu,[1,3,6] M. Ahmad,[1] J.-C. Grivel,[7] R. Scheuermann,[8] M. v. Zimmermann,[9] M. Boehm,[6] P. Steffens,[6] Ch. Niedermayer,[5] K. S. Pedersen,[10] N. B. Christensen,[2] B. O. Wells,[11] K. Lefmann,[1,†] and L. Udby[1]

[1]*Nanoscience Center, Niels Bohr Institute, University of Copenhagen, 2100 Copenhagen Ø, Denmark*
[2]*Department of Physics, Technical University of Denmark, 2800 Kgs. Lyngby, Denmark*
[3]*Department for nanotechnology, Danish Fundamental Metrology, Kogle Allé 5, 2970 Hørsholm, Denmark*
[4]*Department of Physics, Oxford University, Oxford OX1 3PU, United Kingdom*
[5]*Laboratory of Neutron Scattering, Paul Scherrer Institute, 5232 Villigen PSI, Switzerland*
[6]*Spectroscopy Group, Institute Max von Laue Paul Langevin, 38042 Grenoble, France*
[7]*Department of Energy Conversion, Technical University of Denmark, 2800 Kgs. Lyngby, Denmark*
[8]*Laboratory for Muon Spin Spectroscopy, Paul Scherrer Institute, 5232 Villigen PSI, Switzerland*
[9]*High Energy X-Ray Diffraction for Physics and Chemistry, Deutsches Elektronen-Synchrotron DESY, Notkestrasse 85, 22603 Hamburg, Germany*
[10]*Department of Chemistry, Technical University of Denmark, 2800 Kgs. Lyngby, Denmark*
[11]*Department of Physics and Institute of Materials Science, University of Connecticut, Storrs, Connecticut 06269, USA*

(Received 26 January 2021; revised 17 October 2023; accepted 26 April 2024; published 13 May 2024)

We present a combined neutron diffraction and high-field muon spin rotation (μSR) study of the magnetically ordered and superconducting phases of the high-temperature superconductor $La_{1.94}Sr_{0.06}CuO_{4+y}$ [T_c = 37.5(2) K] in a magnetic field applied perpendicular to the CuO_2 planes. We observe a linear field-dependence of the intensity of the neutron diffraction peak that reflects the modulated antiferromagnetic stripe order. The magnetic volume fraction extracted from μSR data likewise increases linearly with applied magnetic field. The combination of these two observations allows us to unambiguously conclude that stripe-ordered regions grow in an applied field, whereas the stripe-ordered magnetic moment itself is field-independent. This contrasts with earlier suggestions that the field-induced neutron diffraction intensity in La-based cuprates is due to an increase in the ordered moment. We discuss a microscopic picture that is capable of reconciling these conflicting viewpoints.

DOI: 10.1103/PhysRevB.109.174517

I. INTRODUCTION

Magnetic fluctuations are the most likely pairing mechanism behind high-temperature superconductivity (SC) in the cuprates [1], and therefore they deserve to be studied in detail. The static antiferromagnetic (AFM) order of the parent Mott insulator compounds prevents SC from occurring. Upon doping, the AFM order is suppressed and SC appears; however, charge-density-wave order, observed by x-ray diffraction studies, also emerges upon doping and is likewise known to compete across several cuprate families with SC [2–4].

The earliest direct evidence of modulated charge and magnetic ordering in cuprate superconductors was the discovery of *stripe* order in hole-doped $La_{2-x-y}Nd_ySr_xCuO_4$ [5] found with neutron diffraction studies and later in $La_{2-x}Ba_xCuO_4$ [6], in $La_{2-x-y}Eu_ySr_xCuO_4$ [7,8], and in $La_{2-x}Sr_xCuO_4$ [9], all of them chemically *a*-site doped La-214 type cuprates.

Another route for introducing holes to the CuO_2 planes is adding excess oxygen to the material, e.g., in $YBa_2Cu_3O_{6+y}$ [10] and La_2CuO_{4+y} [11]. Unlike doping by chemical substitution, the oxygen dopants remain mobile in La_2CuO_{4+y} down to temperatures around 200 K [12–14]. Above this temperature, the holes can distribute in a way that at low temperatures favors long-range-ordered stripe regions with a period of eight unit cells [15] and support connected SC regions to give the highest critical temperature T_c for the La-214 family [14].

In many oxygen stoichiometric La-214 cuprates, stripe order is most prominent at dopings just around $x = 0.125$, accompanied by a suppression of T_c [6,9,16–19]. Here, the intensity of the neutron diffraction (ND) peak from the stripes is enhanced by an applied magnetic field [19–21]. At higher doping levels, the stripe order is absent, but it can be induced by a magnetic field [19,22–24].

The field-driven enhancement of the magnetic ND peak has often been interpreted as a field-induced increase of the ordered moment in La-214 cuprates [19,20,25]. However, studies using neutron diffraction and muon spin rotation (μSR) have revealed that oxygen doped La-214 cuprates exhibit *electronic phase separation* between optimally doped SC without static magnetism and a magnetic stripe ordered

*sonja@nbi.ku.dk
†lefmann@nbi.ku.dk

phase without SC [26–28]. This finding stands in contrast to the suppression of SC found in oxygen stoichiometric La-214 mentioned above.

In codoped $La_{2-x}Sr_xCuO_{4+y}$, holes are introduced both by chemical substitution and by intercalating extra oxygen. So far, stripe order is found in all oxygen codoped samples when they are optimally oxygen-doped, achieving $T_c \approx 40$ K [15,29–31]. In contrast, oxygen-stoichiometric $La_{2-x}Sr_xCuO_4$ shows stripe order only in the underdoped region, $x < 0.135$, with T_c of 30 K or less [19,22,23,27,32].

Detailed transport studies of $La_{1.875}Ba_{0.125}CuO_4$ uncovered evidence for two-dimensional (2D) superconducting correlations developing at the spin-ordering temperature, T_N, in zero field, but becoming rapidly suppressed upon application of a magnetic field perpendicular to the CuO_2 planes [33]. Evidence for electronically decoupled planes associated with stripe magnetic order has likewise been found in optical studies of underdoped, stripe-ordered $La_{2-x}Sr_xCuO_4$ and $La_{2-x-y}Nd_ySr_xCuO_4$ superconductors [34–36]. In the case of $La_{2-x}Sr_xCuO_4$, application of a c-axis magnetic field suppresses the Josephson plasma resonance observed by infrared spectroscopy [35], interpreted as a weakening of the interlayer Josephson coupling. The observations of 2D superconductivity in the cuprates inspired the development of theories for pair-density-wave (PDW) order [37–39] and more broadly the concept of intertwined orders in high-T_c superconductors [40].

It is evident that there is a rich interplay between the 2D SC, the stripe order, both structural and magnetic, and 3D SC in these cuprate compounds, and that there is a need to investigate the different phases in the cuprates in order to understand the competition, interplay, and phase separation of the different states of matter.

In this work, we study the magnetic stripes in codoped $La_{1.94}Sr_{0.06}CuO_{4+y}$. We use μSR to show that there is no static magnetism in our sample, in contrast to $La_{2-x}Sr_xCuO_{4+y}$ compounds with other Sr dopings [29,30]. We further show that an applied magnetic field induces the magnetic order, increasing the magnetic volume fraction linearly from 0% at 0 T to 37(3)% at 8 T. At the same time, the intensity of the ND peak from the stripe order also increases linearly with an applied magnetic field. The combination of these observations implies that the field-induced ND peak is caused solely by the increase in the magnetic volume fraction, while the size of the ordered magnetic moment is field-independent. This is in contrast to some conclusions drawn in earlier studies, where the ordered magnetic moment was found to increase with increasing field [19,20,25].

II. METHODS

A 7.9 g single crystal was grown by the traveling solvent floating zone method and was oxygenated through a wet-chemical technique [29] obtaining a single onset transition temperature of $T_c = 37.5(2)$ K. Magnetization measurements were performed both before and after oxidation; see Appendix A. To ensure consistency between our experiments, the sample was always field-cooled; the sample was heated to at least 50 K (well above T_c and the Néel temperature T_N) before any change of applied magnetic field. We adopted a slow cooling procedure as described in Ref. [13] to allow the oxygen to find an optimal configuration before freezing [14,41]; see Appendix A for details.

ND was performed at the cold triple axis spectrometers RITA-II at Paul Scherrer Institute (PSI), Switzerland [42,43] and ThALES at Institute Laue-Langevin (ILL), France [44–46]. In both ND experiments, the sample was mounted in a 14.9 T cryomagnet with the c-axis along the field. The incoherent elastic energy resolution was ~0.2 meV (full width at half-maximum). The crystal was mounted to allow access to wave vectors $\mathbf{Q} = (h, k, 0)$, expressed in units of $(2\pi/a, 2\pi/b, 0)$ (using orthorhombic notation); see Appendix D for details on the instrument setup. The sample configuration allowed us to measure the peaks from the stripes, which appear as a quartet of weak peaks around the antiferromagnetic point $\mathbf{Q}_{\mathrm{AFM}} = (1, 0, 0)$ [47].

To measure the interplanar magnetic correlations, the sample was mounted with the c-axis in the scattering plane in a horizontal field magnet. The experiment was carried out at the RITA-II spectrometer with the same configuration as described above (and in Appendix D).

The μSR measurements were carried out at the General Purpose Spectrometer [48] and the high transverse field spectrometer HAL9500 [49], both located at PSI. We used a smaller piece of the same sample and applied the magnetic field along the c-axis. See Appendix C for details on the μSR measurements and data analysis.

We performed hard x-ray diffraction experiments at the BW5 beamline at HASYLAB, Deutsches Elektronen-Synchrotron, Hamburg, Germany. Here we looked for a signature of charge-density waves. The sample was cut into a thin slice ($d = 1.4$ mm) in order to reduce the absorption, meaning that 10% of the incoming beam was transmitted through the sample.

The magnetization measurements were carried with the magnetic field applied along the c-axis in a vibrating sample magnetometer (VSM) in a Physical Properties Measurement System (PPMS) located at the Technical University of Denmark.

III. RESULTS

A selection of raw ND data is presented in Fig. 1(a), showing a clear field-induced peak at 14.9 T. The intensity of the peak decreases with decreasing field, but a tiny signal may still be present at 2 K in zero field. However, the error on the fitted amplitude in zero field is nearly as large as the value itself. We fitted the data using Gaussian peaks on a sloping background. Due to the weak signal, not all parameters were fitted simultaneously. The peak center and width show no visible dependence on the magnetic field, and we have thus fixed these to the values obtained at 14.9 T.

The stripe peaks are present at all four scattering vectors $\mathbf{Q}_{\mathrm{stripe}} = (1 \pm \delta_h, \pm\delta_k, 0)$ with $\delta_h \approx \delta_k = 0.124(2)$, and they correspond to a period-8 antiferromagnetic modulation along the Cu-O bonds. The peak located at $(1 + \delta_h, -\delta_k, 0)$ was used for the temperature and magnetic field dependence studies. The full width at half-maximum of the peak is $2w = 0.019(2)$ r.l.u., which is similar to measurements on other La-214 cuprates at similar cold neutron instruments; see, e.g., Ref. [19].

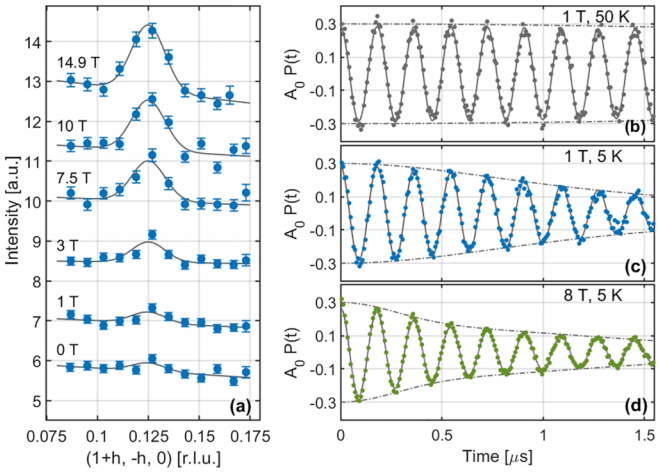

FIG. 1. (a) ND data measured at RITA-II at 1.6 K, counting between 7 and 18 min per point. Each data set is offset by a multiple of 1.5 a.u.. Solid lines are Gaussian fits, as described in the text. (b)–(d) Examples of μSR asymmetry data in applied magnetic fields measured at HAL9500. Solid lines are fits as described in the text, and dashed envelopes highlight the difference in the fitted relaxation rates.

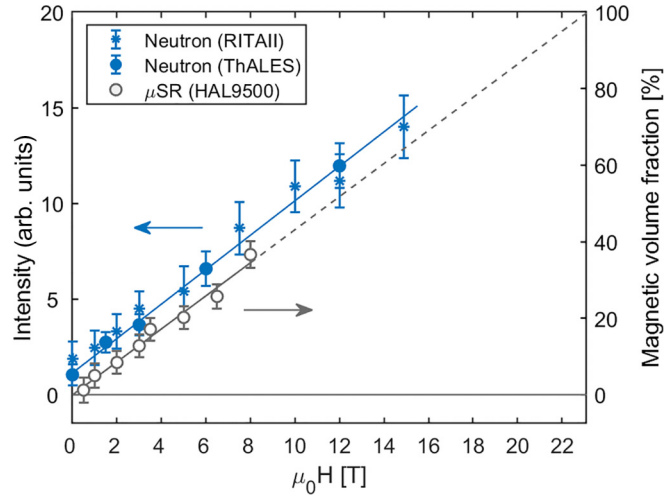

FIG. 2. The low-temperature magnetic field dependence of the neutron diffraction intensity from the stripe phase (blue) and the magnetic volume fraction measured with μSR (gray).

The intrinsic width of the peak (γ) is related to the correlation length of the stripe regions, $\xi_{\mathrm{AFM}} = 1/\gamma$. To determine ξ_{AFM}, we need to account for the instrument resolution, σ. Since the resolution function depends on the scattering angle, the resolution near the forbidden (100) peak cannot be determined experimentally from measurements of other peaks, such as the (200) nuclear Bragg peak [50]. We have therefore estimated the instrument resolution for the particular scan in two ways: (a) simulating an ideal sample using McStas [51], which is known to reproduce linewidths to a precision of a few percent [43,52], yielding $\sigma = 0.0147$ r.l.u., and (b) measuring the second-order scattering on the nominal (100) peak, yielding $\sigma = 0.0170$ r.l.u. From these two estimates, the intrinsic width of the peak is (a) $\gamma = 0.012(3)$ r.l.u. or (b) $\gamma = 0.009(12)$ r.l.u. (i.e., not significantly different from 0). A conservative lower bound on the correlation length of the stripe regions from estimate (a) is $\xi_{\mathrm{AFM}} = 1/\gamma > 14$ nm, while estimate (b) is consistent with long-range order.

Figures 1(b)–1(d) show a selection of μSR asymmetry spectra in a rotating reference frame (RRF) chosen such that the very high muon spin precession frequencies at high fields are scaled down for better visualization of the data. The RRF frequency is 130 MHz at 1 T and 1080 MHz at 8 T. In panel (b), data taken at 50 K show an undamped oscillation of the muon spin asymmetry that is well described by a model including a single Gaussian component with a frequency corresponding to the external magnetic field of 1 T. This behavior is expected for a paramagnetic sample. At 5 K and 1 T in panel (c), the spectrum shows a clear decay of the muon spin asymmetry, which is dominated by one oscillating component with Gaussian relaxation. In panel (d) at 8 T and 5 K, the time evolution of the muon spin asymmetry is best described using two distinct components corresponding to the magnetic and nonmagnetic regions in the sample, respectively. Below, we argue that the nonmagnetic regions of the sample are superconducting. The pronounced rapid decay of the muon asymmetry at early times is modeled by a Gaussian oscillation with an enhanced relaxation rate, consistent with muons stopping in magnetically ordered regions. The magnetic and SC components have rotation frequencies ω_{m} and ω_{SC}, and Gaussian decay parameters σ_{m} and σ_{SC}, respectively. For details on the μSR data treatment, see Appendix C.

Figure 2 shows the main result of this study, namely the linear dependence of the ND intensity and magnetic volume fraction (V_{m}) found with μSR measured at low temperatures (RITA-II at 1.8 K, ThALES at 1.5 K, and HAL9500 at 2.5 K). The linear dependence has been found in two different neutron experiments, and their axes have been scaled independently to have the linear fits coincide on the arbitrary scale. The μSR measurements are on an absolute scale and directly show that the magnetically ordered fraction of the sample scales linearly with applied field.

In Fig. 3 the temperature dependences of parameters found with three different techniques are displayed together. Figure 3(a) shows the integrated intensity of the ND peak measured at ThALES. The magnetic ordering temperature is determined to $T_{\mathrm{N}} = 39(1)$ K for both 6 and 12 T.

Figure 3(b) displays V_{m} as a function of temperature, extracted from the μSR data. The fast relaxation associated with magnetic order vanishes at 40(1) K, consistent with $T_{\mathrm{N}} = 39(1)$ K found with neutrons. Panel (c) shows that the relaxation rate σ_{SC} of the nonmagnetic regions takes a constant value of 0.47 $\mu\mathrm{s}^{-1}$ at higher temperatures. On cooling below 32 K, σ_{SC} increases to reach a value of 0.95(5) $\mu\mathrm{s}^{-1}$ at 2 K. In panel (d) the rotation frequency of the muons in the nonmagnetic regions is seen to be constant at high temperature, with a value that corresponds to the external magnetic field. The small negative shift of ω_{SC} below 38 K together with the increase of σ_{SC} appearing below T_{c} is typical for SC and can be understood in terms of a broadening of the field distribution due to the formation of a flux line lattice within the SC state that forms below T_{c} [53]. We thus ascribe this nonmagnetic component at low temperatures to muons stopping in SC

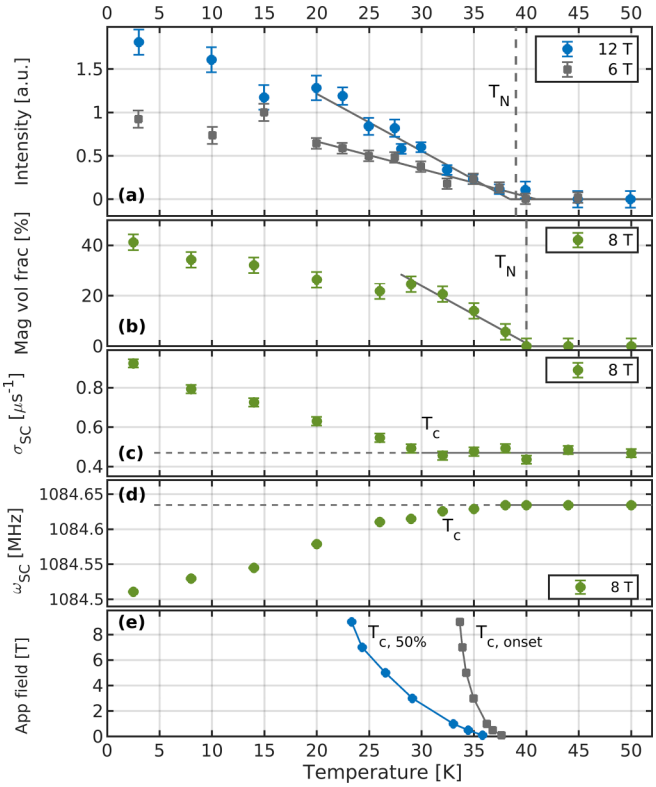

FIG. 3. (a) The intensity of the ND peak as a function of temperature for applied fields of 6 and 12 T. The solid lines are linear fits to the 6 and 12 T data in the range 20–40 K. (b)–(d) μSR fitting parameters determined in 8 T. The solid line in (b) is a linear fit to V_m in the range 30–40 K. The constant lines in (c) and (d) are fits to σ_{SC} and ω_{SC} above 38 K. (e) T_c onset and 50% magnetization point as a function of field, found from field-cooled magnetization measurements.

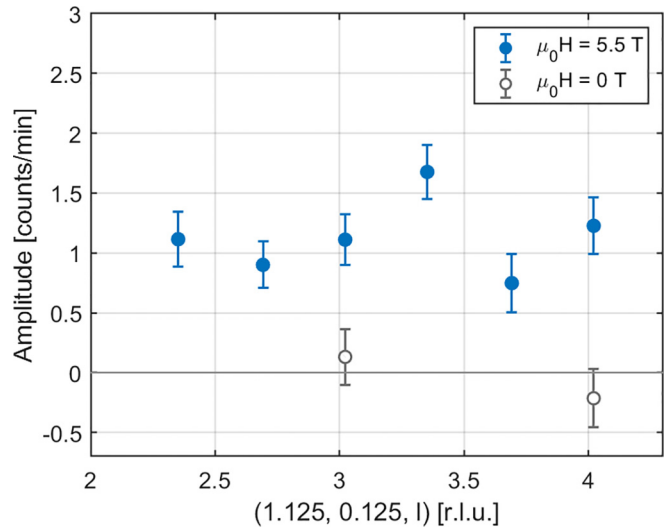

FIG. 4. Neutron diffraction intensities show the two-dimensional nature of the magnetic peak along the l-direction, measured at 2.3 K.

regions of the sample, as done in Refs. [29,30]. There is no evidence of a third component that is simultaneously non-SC and nonmagnetic.

The temperature dependence of the sample magnetization is shown in Fig. 3(e). We measured for seven different field values in the range 0.1–9 T. The transition from the normal to the SC state broadens drastically with applied field. The raw data and fits are shown in Fig. 7 in Appendix B. We determine the onset of the SC transition $T_{c,onset}$ as well as the 50% magnetization point $T_{c,50\%}$ as a function of field with linear fits to the magnetization data; see Fig. 7 in Appendix B. From the field dependence of T_c in low fields, it is possible to give an estimate of the critical field, $H_{c2}(0)$, and thereby the superconducting coherence length, ξ, using the Werthamer-Helfand-Hohenberg (WHH) model. This crude estimate gives $H_{c2}(0) \approx 17$–54 T and $\xi \sim 2.5$–4.5 nm in agreement with other dopings of $La_{2-x}Sr_xCuO_4$ [54]. See Appendix B for details on the WHH model.

In Fig. 4 the l-dependence of the amplitude of the magnetic peak is shown. Sample rotation scans were performed above T_N and subtracted as background from the low-temperature data at 2.3 K. This procedure was performed in zero field and in an applied field of 5.5 T. The data were binned with a step size of 0.3 r.l.u. along l. Due to the mismatch between the poor out-of-plane resolution of a triple-axis instrument and the rodlike signal along l from the magnetic scattering, it is extremely difficult to get adequate statistics for this experiment. Moreover, the maximum field strength of the horizontal field magnet is 5.5 T, and only about 20% of the sample is in the magnetic phase at this field. With a counting time of 48 min per point, it was only possible to extract the amplitudes of Gaussian fits with fixed values of the width and center (the background is zero due to the subtraction). Under these conditions, the data show a field-induced magnetic signal but no intensity modulation along l.

We searched for a field-induced x-ray diffraction signal at $(\pm 0.25, \pm 0.25, l)$ for several values of $l = 8$, 8.25, 8.5, 9.5, 11.5, and 12.5 in an applied field of 10 T. Even with an extreme counting time of up to 7.5 min per point, no signal was found. Figure 5 shows an example of our raw data.

IV. DISCUSSION

The onset of the magnetic signal is found, within error, at the same temperature, independent of applied field (6, 8, and 12 T) measured with both ND and μSR; see Figs. 3(a) and 3(b). At 8 T, the SC transition (T_c onset) found with magnetization measurements coincides with the onset temperature found by μSR at 8 T as seen in Fig. 3(e) compared to Figs. 3(c) and 3(d). At low fields, the SC and magnetic phases have the same transition temperature, but at higher fields the two transition temperatures differ from each other, as T_N remains unchanged while T_c is suppressed with field. This result is consistent with findings in $La_{2-x}Sr_xCuO_4$ with $x = 0.10$ having $T_N \sim T_c(H = 0) = 30$ K [20]. While the similarity of T_N and T_c at low fields might be seen as an indication of one correlated phase, we interpret the different onset temperatures at higher field values as a signature of two competing phases—magnetic and SC—with almost degenerate free energy in zero field. The application of a magnetic field favors the formation of regions with quasistatic stripe order and suppresses T_c.

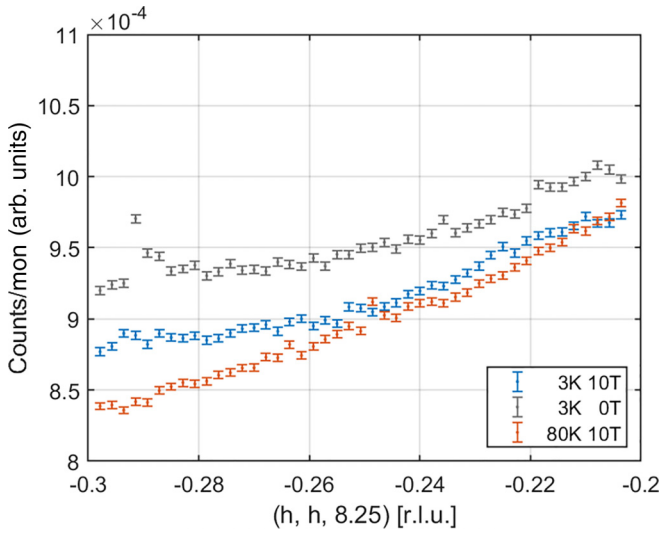

FIG. 5. Examples of the raw data from the x-ray diffraction experiments. No field-induced diffraction peak indicating charge density waves can be found in the data measured at 3 K and 10 T (gray points).

Extrapolating our μSR results to higher fields in Fig. 2, V_m reaches 100% at $B_{sat} \sim 23$ T, suppressing the SC phase completely. This is consistent with our crude estimate of $H_{c2}(0) \approx 17$–54 T from the WHH model. This further indicates that the magnetic stripe phase and SC competes. It is, however, remarkable that we find no evidence of charge stripes of the type observed in other La-214 compounds, even though we used the exact same method as in Refs. [55,56]. This finding is consistent with a picture of magnetic fluctuations rather than static magnetic (and structural) order. In Ref. [57] it is discussed how the formation of static charge stripes happens, and that the relationship between charge nematicity and the magnetic stripe signal may not be simple.

In zero field, a tiny ND signal seems to be present, while no static magnetism is observed with μSR. The small discrepancy between the results may be explained by the difference in timescale between the two techniques. Cold neutron measurements probe a timescale of $\sim 10^{-11}$ s and cannot distinguish fluctuations on longer timescales from static magnetism. In contrast, high transverse field μSR measurements probe a timescale of $\sim 10^{-7}$ s. Magnetic moments fluctuating on a timescale between these two values would thus be seen as static by the neutrons, but as fluctuating by the muons. The difference between the two techniques may thus be reconciled if the stripe signal is not truly static, but rather slow fluctuations, as discussed, e.g., in Refs. [21,58,59]. Therefore, the peak at 0 T likely does not originate from truly static moments, but low-energy fluctuations picked up by the finite energy resolution of the instrument.

The ND peak at low temperature increases linearly with magnetic field; see Fig. 2. The measured ND intensity scales as $I \propto V_m M_\perp^2$, where V_m is the magnetic volume fraction and $M_\perp$ is the component of the ordered moment perpendicular to the scattering vector [50]. At the same time, our μSR experiments show a pure SC phase at zero field and a linear increase of V_m with applied field. Combining the results of the two techniques, constituting a local probe and a coherent probe, we conclude that the observed increase in the ND signal is caused purely by an increase in V_m, and not by an increase of $M_\perp$.

Previous ND investigations of $La_{2-x}Sr_xCuO_4$ in samples that exhibit near 100% magnetic volume fraction in zero field [19,60] found a field-enhanced intensity, which was ascribed to an increase in the ordered moment of preexisting magnetic order. A similar interpretation was presented for La_2CuO_{4+y} in Ref. [25]. In contrast, the linear increase in the magnetic scattering intensity in our sample can be fully accounted for by the linear increase in the magnetic phase fraction derived from the muon signal, leaving no evidence for an increase in the size of the local moments. This raises an apparent contradiction. While the phenomenology of the field-enhanced scattering in the two systems seems incompatible with a single mechanism, it seems unlikely that the effect of a magnetic field in two such similar La-214 systems is fundamentally different. Below we present an interpretation of the available data, which allows for a single description favoring the phase fraction description.

There are only a few studies of the field-dependent magnetic scattering that include both μSR and neutron diffraction data. This makes it difficult to construct a direct connection between phase fractions and the magnetic scattering intensity. An exception is the combined ND and μSR study of $La_{2-x}Sr_xCuO_4$ samples of $x = 0.105$, 0.12, and 0.145 in Ref. [19]. Of particular note is the $La_{2-x}Sr_xCuO_4$ sample with $x = 0.12$, which shows significant field enhanced scattering but near 100% magnetic phase fraction even in zero field. However, μSR does not measure local moments directly, but rather the local magnetic field, which is influenced by moments arrayed over a range of around 10–20 Å. Reference [19] notes that the magnetic structure of the $x = 0.12$ sample may be inhomogeneous at this lengthscale.

Thus, a possible connected picture emerges. In the $La_{2-x}Sr_xCuO_{4+y}$ sample reported here, phase separation creates large magnetic and SC regions, and the application of a magnetic field increases the magnetic volume fraction in a straightforward manner. In the $La_{2-x}Sr_xCuO_4$ sample with $x = 0.12$, a frustrated tendency towards phase separation leads to inhomogeneity on a subnanometer scale. Application of a field again favors the formation of the striped magnetic region, but in this case the induced stripe phase fills the spatial gaps between existing striped regions, creating a more homogeneous phase and larger local fields at the muon sites.

A similar explanation of a field-induced shift in balance between the volume of two competing volume fractions could be relevant also for the superconductor $YBa_2Cu_3O_{6+y}$, where $T_N \simeq T_c$ and a linear field dependence of the magnetic neutron diffraction peak is observed [61].

In general, there is experimental evidence that magnetic stripes coexist with SC in the La-214 materials [4,5,55,56], but it remains unknown if the coexistence is microscopic or not. The superconducting coherence length in this sample has been estimated via the WHH model to be in the range $\xi = 2.5$–4.5 nm, which is in agreement with other $La_{2-x}Sr_xCuO_4$ compounds, e.g., Ref. [54]. We find the lower limit of the magnetic correlation length to be

significantly larger, $\xi_{AFM} > 14$ nm. These findings suggest that the field-induced stripe order is correlated beyond the size of a vortex core, in agreement with, e.g., Ref. [20]. Therefore, the simple picture that magnetism is found only inside the vortex core is inadequate, and further investigations of the overlap between the magnetic and SC phases are needed.

When discussing domain sizes, it is important to note that these systems are somewhat two-dimensional in nature. There is a striking parallel between the phenomenology of broken interlayer Josephson coupling detected optically, and that of the field dependence of stripe magnetic order detected by neutron diffraction: When stripe order is well-developed and T_c strongly suppressed, as in the case of $La_{2-x}Ba_xCuO_4$ and $La_{2-x-y}Nd_ySr_xCuO_4$ near $x = 1/8$, 2D superconducting correlations are detected in zero magnetic field [36], while the incommensurate stripe magnetic order is field-independent [19,62]. On the other hand, stripe order is less well-developed under zero-field conditions in underdoped $La_{2-x}Sr_xCuO_4$, and T_c is correspondingly less suppressed. In this family of materials, diffraction studies indicate field-enhanced Bragg peak intensities [19,20], and as stripe order strengthens, optical studies indicate a gradual emergence of 2D superconductivity [35,36]. It therefore appears that stripe order and 2D superconducting correlations go hand in hand.

The intensity of the ND signal from magnetic stripes shows no or little variation along the out-of-plane l-direction. This demonstrates that the field-induced magnetic peak in our sample is two-dimensional, different from the zero-field magnetic signal in $La_{2-x}Sr_xCuO_4$ where short-ranged magnetic correlations along the c-axis were found for $x = 0.10$ [63] and $x = 0.12$ [60]. Also in La_2CuO_{4+y}, pronounced modulations along l have been found [15]. It is, however, possible that any modulation of the neutron signal from a single (magnetic) domain could be washed out, and thus remain unobserved, due to a scattering signal from other magnetic domains (e.g., due to twinning in the crystal) with large intensity at different l-values [60]. Thus, observation of (short-range) magnetic c-axis correlations could depend on systematic or accidental detwinning of particular samples.

Some of us have studied other codoped samples of $La_{2-x}Sr_xCuO_{4+y}$ with values of the Sr-doping x being 0.04, 0.065, 0.09, and 0.115. For the sample with $x = 0.09$, we found no field-enhancement of the ND stripe signal [64]. This could suggest that parts of the $x = 0.09$ sample would display 2D superconductivity, while other parts would be stripe-free and 3D superconducting.

The magnetic volume fraction in zero field for codoped samples with different Sr content varies between 20% and 65% [29]. Our sample, however, has no magnetic volume fraction in zero magnetic field. One can speculate that our sample is positioned at the crossover point between annealed order (O-doping) and quenched disorder (Sr-doping). This would mean that the local doping is so evenly distributed that there is no spatial variation that favors magnetic domain formation. A systematic study of this effect could be interesting.

V. CONCLUSION

In conclusion, by combining neutron diffraction, muon spin rotation, and magnetization measurements in strong magnetic fields, we have found that $La_{2-x}Sr_xCuO_{4+y}$ with $x = 0.06$ shows no magnetic order at low temperature, and that the application of a magnetic field induces stripe ordered regions. The volume of these regions is proportional to the applied field value, while the ordered magnetic moment is field-independent. These findings are in contrast to the interpretation of earlier, similar data on field-induced magnetism in oxygen-stoichiometric $La_{2-x}Sr_xCuO_4$ samples, where a field-induced enhancement of neutron diffraction intensity was interpreted to be caused by an increase in the ordered magnetic moment. Our results make it relevant to reinvestigate with μSR whether the field-enhanced stripe signal in the other La-214 cuprates is due to an increase of the ordered moment, as previously concluded, or rather caused by an increased magnetic volume fraction. The answer to this is highly relevant for the understanding of the interplay between magnetism and SC in the cuprate superconductors.

When comparing with similar studies of other $La_{2-x}Sr_xCuO_{4+y}$ samples with different values of the Sr doping, x, we find that our value, $x = 0.06$, presents the perfect balance of quenched disorder doping and the annealed ordered doping of mobile oxygen in order to avoid static stripes from forming in zero magnetic field. If the sketched equivalence of phenomenologies is correct, then what our sample provides is a clean laboratory for studying the competition between 2D superconducting, stripe-order (field induced) and 3D superconducting, stripe-free regions.

ACKNOWLEDGMENTS

This work is based on experiments performed at the Swiss Neutron Source SINQ and Muon Source SμS, Paul Scherrer Institute, Villigen, Switzerland. We also thank the Institut Laue-Langevin (ILL), France for providing neutron beam time. We acknowledge DESY (Hamburg, Germany), a member of the Helmholtz Association HGF, for the provision of experimental facilities. We would like to thank Dr. Tatsuo Goko (PSI) for assistance during the μSR experiment, and Prof. Dr. Kazimierz Conder (PSI) for performing TGA measurements. The work has been supported by the Independent Research Fund Denmark, Project 0602-01982B. We thank the Danish Agency for Science, Technology, and Innovation for funding the instrument center DanScatt. Grant No. 7129-00006B. S.H.D. has been funded by NordForsk through NNSP, Project No. 87865, and by the Carlsberg Foundation CF19-0697. H.J. was funded by the EU Horizon 2020 program under the Marie Sklodowska-Curie Grant Agreement No. 701647 and the Carlsberg Foundation CF20-0497. B.O.W. was supported for sample production and data interpretation by the U.S. DOE-BES under Contract No. DE-FG02-00ER45801.

APPENDIX A: SAMPLE SYNTHESIS AND CHARACTERIZATION

A large single crystal was grown at the Department of Energy Conversion and Storage, Technical University of Denmark, in a mirror furnace using the traveling solvent floating zone method. After cutting, we obtained a 20-mm-long cylinder with a diameter of 10 mm and a mass of $m = 7.9$ g.

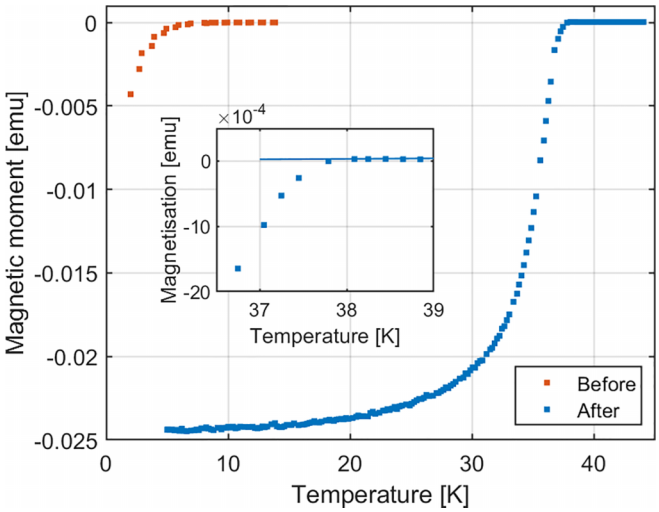

FIG. 6. Magnetic moment measured before and after oxygenation in an applied field of 20 Oe. The inset is a zoom-in of the data measured after oxygenation, from which we obtain the low-field onset critical temperature of $T_c = 37.5(2)$ K.

The nominal Sr content of the material (from the mixing of powders preceding the growth of the single crystal) was $x = 0.06$.

We measured the magnetic response of a small piece of the as-grown sample using an ac magnetic susceptometer setup and found a diamagnetic signal below ∼6 K, as shown with red dots in Fig. 6. This value of the critical temperature is consistent with other Sr-doped samples with $x \sim 0.06$ [65,66]. The sample was oxygenated at the University of Connecticut through a wet-chemical technique for several months [29]. The rod was cut into pieces to fit it in the cryomagnets used in the neutron experiments. A small piece of oxygenated sample was measured with a VSM in an applied field of 20 Oe. It reveals a single transition for our $La_{1.94}Sr_{0.06}CuO_{4+y}$ sample, shown in Fig. 6 in blue dots.

At low temperatures the sample is orthorhombic, and we found $a \simeq b = 5.33$ Å and $c = 13.15$ Å. The most likely structure is low-temperature orthorhombic, space group *Bmab* [67], but multiple other space groups are possible depending on the exact nature of the oxygen octahedral tilts [68].

Oxygen mobility and cooling rates

Excess oxygen has been shown to be mobile in $La_{2-x}Sr_xCuO_{4+y}$, and, e.g., quench cooling of the sample from 200 or 300 K yields very different low-temperature properties from after slow cooling [14,41]. For this reason, all our experiments reported were performed using a slow cooling rate (1 K/min or lower) from room temperature to 100 K in order to provide consistency between measurements, and to make sure the mobile excess oxygen ions find an optimal configuration in the crystal structure before freezing.

APPENDIX B: MAGNETIZATION MEASUREMENTS AND THE SUPERCONDUCTING PHASE

In Fig. 7, we display the measured magnetization for different applied fields. The magnetic response of the sample at low temperatures is dominated by diamagnetism due to the superconducting phase for all applied fields in this study ($B \leqslant 9$ T).

The precise determination of a single T_c is made difficult by thermal fluctuations [69] that broaden the transition from the normal state to the superconducting state. We have therefore used two different methods to obtain a measure of T_c as a function of applied field. The first method is to find the halfway point between the full diamagnetic response and the normal state response [70,71]. The open circles in Fig. 7 indicate this 50% magnetization point for each field. In the second approach, we have performed a linear fit to the sloping part of the magnetization curves and found the intersection to the high-temperature magnetization line as our onset temperature, T_{onset}. In Fig. 8, both T_{onset} and the 50% magnetization points are plotted as a function of applied magnetic field.

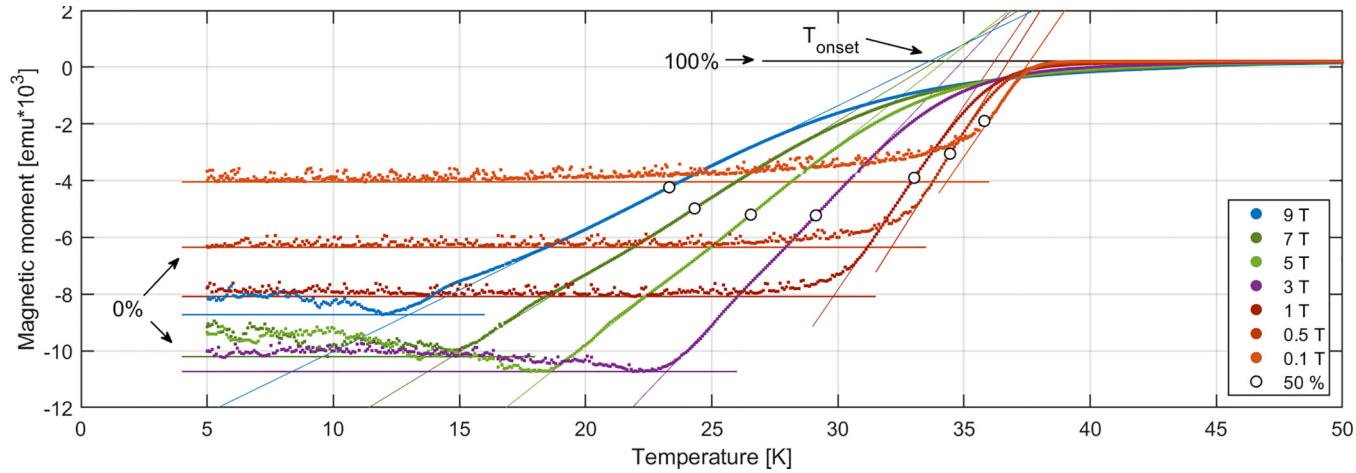

FIG. 7. Magnetic moment measured at different magnetic fields applied along the c-direction. The black line is a fit to the constant region above 50 K. The open circles indicate the 50% magnetization point between the lowest point measured and the high-temperature constant value. The horizontal colored lines mark the lowest value obtained for each magnetization curve. Straight line fits are performed to the linear part of the slopes to obtain a value for T_{onset}.

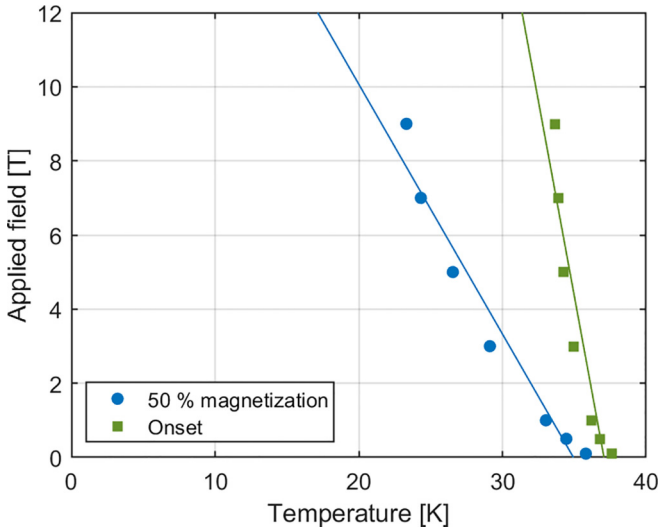

FIG. 8. T_c onset and 50% magnetization point as a function of field, found from magnetization measurements in Fig. 7. These are the same data as displayed in Fig. 3(e) but here with the linear fits of the WHH model.

Werthamer-Helfand-Hohenberg model

The Werthamer-Helfand-Hohenberg theory for type-II superconductors can be used to estimate the upper critical field at zero temperature, $H_{c2}(0)$, from the slope of H_{c2} as a function of temperature [72]. For simplicity, we restrict our analysis to the dirty limit, where [72,73]

$$H_{c2}(0) = -0.69 T_c \frac{dH_{c2}}{dT}. \tag{B1}$$

Typical values for $-dH_{c2}/dT$ in $La_{2-x}Sr_xCuO_4$ are 0.5–1.5 T/K, e.g., Ref. [71].

Using Ginzburg-Landau theory, the superconducting coherence length, ξ, can be estimated using [74]

$$H_{c2}(0) = \frac{\Phi_0}{2\pi\xi^2}, \tag{B2}$$

where $\Phi_0 = 2.06 \times 10^{-15}$ Wb.

Using the halfway point of the magnetization curves to estimate H_{c2}, we find $-dH_{c2}/dT = 0.67(9)$ T/K and $T_{c,50\%} = 35.8$ K in our sample, giving $H_{c2}(0) = 17(2)$ T and $\xi = 4.5(6)$ nm. Using the onset of diamagnetism as an estimate of H_{c2}, we find $-dH_{c2}/dT = 2.1(3)$ T/K and $T_{\text{onset}} = 37.6$ K, and thus $H_{c2}(0) = 54(8)$ T and $\xi = 2.5(4)$ nm. This estimate of $H_{c2}(0)$ is likely an overestimate, as suggested by Ref. [73]. The lines in Fig. 8 show the fits to the WHH model.

We conclude that the superconducting coherence length is between 2.5 and 4.5 nm, assuming that the WHH model can describe our system. This estimate is, in itself, not self-consistent with the dirty limit approximation of the WHH model, where the superconducting coherence length should be larger than the mean free path of the electrons, which for $La_{2-x}Sr_xCuO_4$ is of the order 10 nm [75]. For more precise results, a measurement of $H_{c2}(0)$ is required. Such measurements are outside the scope of this work. We note, however, that our estimates of $H_{c2}(0)$ are in agreement with measurements of $H_{c2}(0)$ in a broad range of LSCO samples [54].

APPENDIX C: MUON SPIN ROTATION

With the μSR technique, the time-dependent decay of an ensemble of muons is measured. The muons enter the sample, and in $La_{2-x}Sr_xCuO_4$ they reside at one unique interstitial lattice site, which makes μSR a local probe that is sensitive to magnetic fields down to 10 μT inside the sample [53]. The positive muons are initially completely spin-polarized, and after implantation they precess in the local magnetic field with a gyromagnetic ratio of $\gamma_\mu = 2\pi \times 135.5$ MHz/T. Muons are unstable particles, and they decay into a positron and a neutrino-antineutrino pair with a lifetime of $\tau_\mu = 2.2$ μs. The positron is emitted preferentially along the direction of the muon spin, and the recorded decay positron count rate thus monitors the spin precession corresponding to the magnetic field strength at the muon site. The μSR spectra obtained in zero-field conditions cover a time window of about 10^{-6}–10^{-9} s, which means that magnetic fluctuations faster than this are averaged to zero, while magnetic fluctuations slower than this are perceived as being static. The average muon implantation depth is of the order 100 μm, and hence the magnetic and superconducting properties measured with muons are representative of the bulk sample.

We carried out two μSR experiments at the SμS facility at the Paul Scherrer Institute (CH), as described below.

1. Zero-field μSR measurements

A zero-field experiment was performed on the GPS spectrometer. We used the forward (in front of the sample) and backward (behind the sample) detector with respect to the muon beam direction to derive the muon spin asymmetry, defined as

$$A(t) = \frac{N^{\text{f}}(t) - \alpha N^{\text{b}}(t)}{N^{\text{f}}(t) + \alpha N^{\text{b}}(t)}, \tag{C1}$$

where α is a scaling factor to account for different efficiency and solid angle coverage of the two detectors.

Figure 9 shows ZF-μSR data measured at 5 K, fitted by a Gaussian Kubo-Toyabe (KT) function:

$$A(t) = \tfrac{1}{3} + \tfrac{2}{3}(1 - \sigma^2 t^2)\exp(-\sigma^2 t^2/2). \tag{C2}$$

From this we find $\sigma = 0.168(1)\,\mu\text{s}^{-1} \sim \gamma_\mu \Delta$, where Δ is the second moment of the magnetic field distribution at the muon site [76]. A Gaussian KT function models the relaxation of muons stopping in a nonmagnetic environment with static and randomly oriented nuclear moments. There is a slight deviation between data and model for long decay times (>6 μs), which indicates that the moments may be fluctuating slightly or that the system is not completely disordered, in agreement with the neutron diffraction data shown in the main paper.

2. High transverse field μSR measurements

In this work, we used the unique possibility of the HAL9500 instrument to apply a magnetic field up to 8 T to the sample. The instrument has eight detectors in front of the sample position and eight detectors behind. The muon

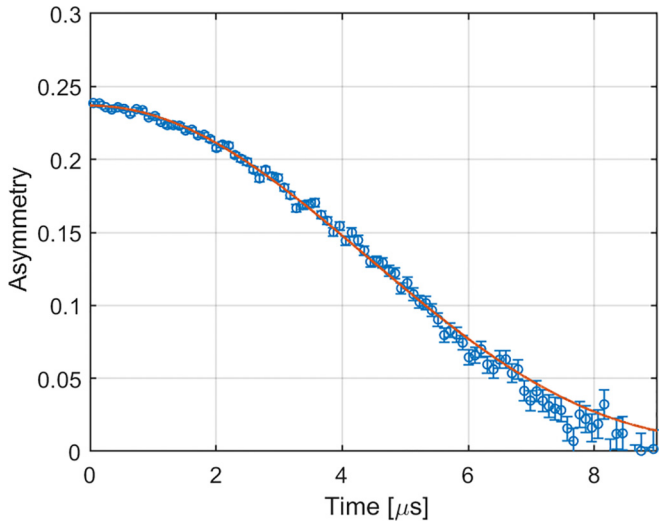

FIG. 9. μSR spectrum recorded under zero-field conditions at 5 K. The red line is the result from a Gaussian Kubo-Toyabe-function fitted to the data.

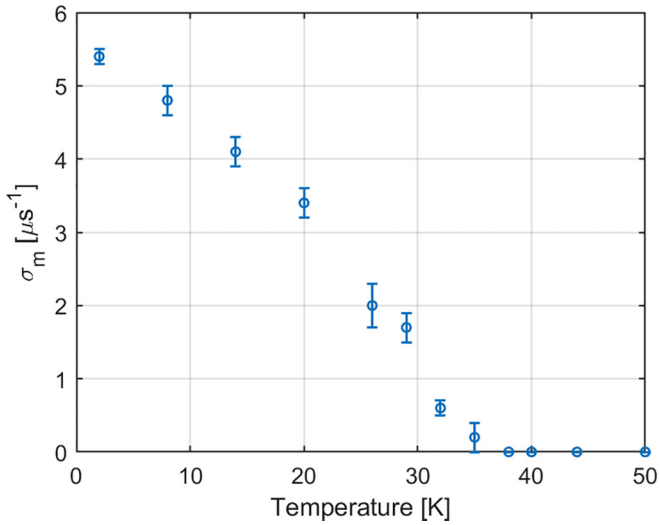

FIG. 10. The relaxation rate of the magnetic regions of the sample as a function of temperature [see Eq. (6)]. The sample was cooled in an applied field of 8 T.

precession phase, normalization, and background counts of each detector are fitted separately, while the key parameters of the model (asymmetry, relaxation rates, and oscillation frequency) are shared between all detectors. The positron count rate in each detector is therefore fitted to the following function:

$$N^i(t) = N_0^i \exp(-t/\tau_\mu)[1 + A(t)] + N_{\rm bg}^i, \qquad \text{(C3)}$$

where $N^i(t)$ is the number of positrons detected at time t in detector i, and N_0^i and $N_{\rm bg}^i$ are the initial number of positrons and the background count in the detector, respectively. From the asymmetry function, $A(t)$, physical parameters such as strength and distribution of the magnetic field within the sample can be extracted from fits to the models presented below.

The high transverse field μSR data have been fitted with a two-component model with the following function represented in a rotating reference frame:

$$A(t) = V_{\rm m} \exp\left(-\sigma_{\rm m}^2 t^2/2\right) \cos(\omega_{\rm m} t + \phi^i) + (1 - V_{\rm m}) \exp\left(-\sigma_{\rm SC}^2 t^2/2\right) \cos(\omega_{\rm SC} t + \phi^i), \qquad \text{(C4)}$$

where $\omega_{\rm m}$ and $\omega_{\rm SC}$ are the Larmor frequencies of the muon spin, and $\sigma_{\rm m}$ and $\sigma_{\rm SC}$ are the second moments of the magnetic field distribution at the muon site. We denote the magnetically ordered (superconducting) regions with the subscript m (SC). The magnetic volume fraction of the sample is parametrized by $V_{\rm m}$. ϕ^i is the initial phase of the muon spin, determined by the detector geometry.

In general, a fast relaxation of the μSR spectrum due to magnetic correlations is analyzed using a model with an exponential envelope. However, for simplicity we have chosen a model where both signals are fitted with Gaussian components. This choice does not affect our results or their interpretation.

A selection of raw data and fits, shown in rotating reference frames, can be found in Figs. 1(b)–1(d). We performed a temperature dependence study with an applied field of 8 T, and a field dependence study at 5 K.

In Fig. 10 the magnetic relaxation rate is shown as a function of temperature in an applied field of 8 T. The relaxation rate decreases as a function of temperature and reaches zero at $T_{\rm N}$. The other three fitting parameters ($\sigma_{\rm SC}$, $\omega_{\rm SC}$, and $V_{\rm m}$) can be found in Figs. 3(b)–3(d). $\omega_{\rm m}$ was held constant at 1084.63 MHz in the constant applied field.

Figure 11 shows the fitting parameters as a function of applied field measured at 2.5 K. The rotation frequencies for the two regions of the sample, $\omega_{\rm m}$ and $\omega_{\rm SC}$, both display a linear field dependence with a slope of 135.5 MHz/T as seen in Figs. 11(a) and 11(c). The magnetic relaxation rate at 2.5 K, $\sigma_{\rm m}$, shows a constant value close to 4.5 μs^{-1} at high fields, but displays a slight upturn at low magnetic fields, Fig. 11(b). The superconducting relaxation rate, $\sigma_{\rm SC}$, varies little with field and has an average value close to 1 μs^{-1}. The small fluctuations around this value are caused by systematic uncertainties.

APPENDIX D: NEUTRON DIFFRACTION

Neutron diffraction was performed at the cold-neutron triple axis spectrometers RITA-II at the Paul Scherrer Institute (PSI), Switzerland and ThALES at Institut Laue-Langevin (ILL), France. With a constant final energy of 5.0 meV, the elastic energy resolution of the two experiments was close to 0.2 meV FWHM, while the **q**-resolution was around 0.025 and 0.015 r.l.u. FWHM at ThaLES and RITA-II, respectively.

RITA-II was configured in the monochromatic imaging mode [42,43], giving an effective collimation of 40′ after the sample. No collimation was used before the sample. No collimation was used on ThALES, but the analyzer geometry was unfocused (flat), and a boron-containing shielding was mounted to cover all but the central analyzer crystal in order to enhance the signal-to-noise ratio. In both experiments, a Be-filter was placed between sample and analyzer to filter out neutrons from second-order scattering.

In the RITA-II experiment, the scans were performed along the $(1 + h, -h, 0)$-direction in reciprocal space, which

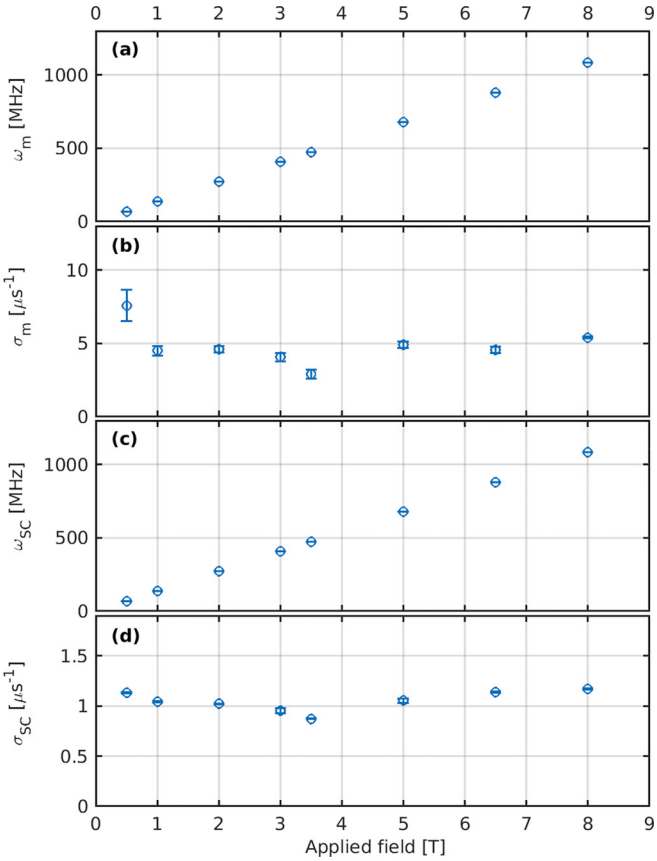

FIG. 11. Parameters found from the two-component fits [Eq. (C4)] as a function of applied field. A plot of V_m vs field can be found in Fig. 2. The sample was heated and field-cooled to 2.5 K for each value of the field.

requires a small adjustment of scattering angle (A4) for each point of the scan. In contrast, in the ThALES experiment, we minimized the variations in the background by doing pure sample-rotation (A3) scans. Here, the scan direction is along a (slightly) curved path in reciprocal space, but there is no change in the scattering angle (A4).

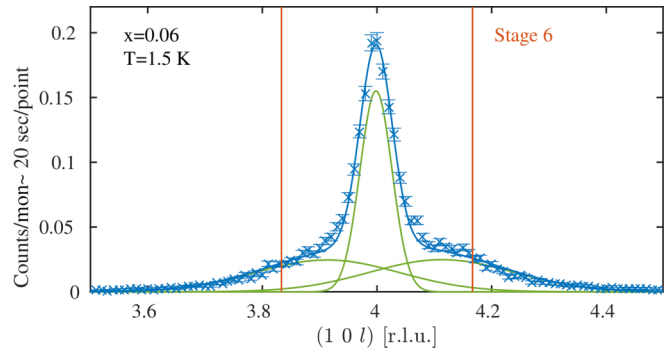

FIG. 12. Neutron diffraction scan along l, centered at the Bragg peak $\mathbf{q} = (104)$. The signal from the ordering of the tilted octahedra appears on either side of the Bragg peak. The data are fitted by the sum of three Gaussians (blue line): one central peak and two broad satellites (green lines). The red lines indicate the position of the stage-6 peaks at $l = 4 \pm 1/6$.

Structural modulation: Staging

The excess oxygen atoms cause anti-phase boundaries of the CuO_6 octahedra tilt pattern along the c-axis, usually denoted as "staging" due to the similarity of intercalated (staged) graphite [77]. The periodicity of these tilt patterns can be observed as (pairs of) superstructure peaks when scanning through *Bmab*-allowed peaks along l, as shown in Fig. 12. Earlier, we showed that the (main) staging peak position shifts closer to the *Bmab* position with increasing Sr content of the $La_{2-x}Sr_xCuO_{4+y}$ samples, indicating larger periodicity of the antiphase tilts [67]. Apart from the *Bmab* peak, we observe two broad peaks centered at $(0, 1, 4 \pm 0.17)$ in our sample. The positions correspond to a modulation of stage-6 or larger. The width of the peaks indicates a distribution of tilt-pattern periodicities with other stage values.

[1] D. J. Scalapino, A common thread: The pairing interaction for unconventional superconductors, Rev. Mod. Phys. **84**, 1383 (2012).

[2] G. Ghiringhelli, M. Le Tacon, M. Minola, S. Blanco-Canosa, C. Mazzoli, N. B. Brookes, G. M. De Luca, A. Frano, D. G. Hawthorn, F. He, T. Loew, M. Moretti Sala, D. C. Peets, M. Salluzzo, E. Schierle, R. Sutarto, G. A. Sawatzky, E. Weschke, B. Keimer, and L. Braicovich, Long-range incommensurate charge fluctuations in (Y,Nd)$Ba_2Cu_3O_{6+x}$, Science **337**, 821 (2012).

[3] J. Chang, E. Blackburn, A. T. Holmes, N. B. Christensen, J. Larsen, J. Mesot, R. Liang, D. A. Bonn, W. N. Hardy, A. Watenphul, M. v. Zimmermann, E. M. Forgan, and S. M. Hayden, Direct observation of competition between superconductivity and charge density wave order in $YBa_2Cu_3O_{6.67}$, Nat. Phys. **8**, 871 (2012).

[4] V. Thampy, M. P. M. Dean, N. B. Christensen, L. Steinke, Z. Islam, M. Oda, M. Ido, N. Momono, S. B. Wilkins, and J. P. Hill, Rotated stripe order and its competition with superconductivity in $La_{1.88}Sr_{0.12}CuO_4$, Phys. Rev. B **90**, 100510(R) (2014).

[5] J. M. Tranquada, B. J. Sternlieb, J. D. Axe, Y. Nakamura, and S. Uchida, Evidence for stripe correlations of spins and holes in copper oxide superconductors, Nature (London) **375**, 561 (1995).

[6] M. Fujita, H. Goka, K. Yamada, J. M. Tranquada, and L. P. Regnault, Stripe order, depinning, and fluctuations in $La_{1.875}Ba_{0.125}CuO_4$ and $La_{1.875}Ba_{0.075}Sr_{0.050}CuO_4$, Phys. Rev. B **70**, 104517 (2004).

[7] M. Hücker, G. D. Gu, J. M. Tranquada, M. v. Zimmermann, H.-H. Klauss, N. J. Curro, M. Braden, and B. Büchner, Coupling of stripes to lattice distortions in cuprates and nickelates, Physica C **460-462**, 170 (2007).

[8] J. Fink, E. Schierle, E. Weschke, J. Geck, D. Hawthorn, V. Soltwisch, H. Wadati, H.-H. Wu, H. A. Dürr, N. Wizent, B. Büchner, and G. A. Sawatzky, Charge ordering in

$La_{1.8}Eu_{0.2}Sr_xCuO_4$ studied by resonant soft x-ray diffraction, Phys. Rev. B **79**, 100502(R) (2009).

[9] T. Suzuki, T. Goto, K Chiba, T Shinoda, T. Fukase, H. Kimura, K. Yamada, M. Ohashi, and Y. Yamaguchi, Observation of modulated magnetic long-range order in $La_{1.88}Sr_{0.12}CuO_4$, Phys. Rev. B **57**, R3229(R) (1998).

[10] Z. Z. Wang, J. Clayhold, N. P. Ong, J. M. Tarascon, L. H. Greene, W. R. McKinnon, and G. W. Hull, Variation of superconductivity with carrier concentration in oxygen-doped $YBa_2Cu_3O_{7-y}$, Phys. Rev. B **36**, 7222(R) (1987).

[11] B. O. Wells, Y. S. Lee, M. A. Kastner, R. J. Christianson, R. J. Birgeneau, K. Yamada, Y. Endoh, and G. Shirane, Incommensurate spin fluctuations in high - transition temperature superconductors, Science **277**, 1067 (1997).

[12] X. Xiong, P. Wochner, S. C. Moss, Y. Cao, K. Koga, and N. Fujita, Evidence of in-plane superstructure formation in phase-separated and staged single crystal La_2CuO_{4+d}, Phys. Rev. Lett. **76**, 2997 (1996).

[13] Y. S. Lee, F. C. Chou, A. Tewary, M. A. Kastner, S. H. Lee, and R. J. Birgeneau, Neutron scattering study of the effects of dopant disorder on the superconductivity and magnetic order in stage-4 La_2CuO_4, Phys. Rev. B **69**, 020502(R) (2004).

[14] M. Fratini, N. Poccia, A. Ricci, G. Campi, M. Burghammer, G. Aeppli, and A. Bianconi, Scale-free structural organization of oxygen interstitials in La_2CuO_{4+y}, Nature (London) **466**, 841 (2010).

[15] Y. S. Lee, R. J. Birgeneau, M. A. Kastner, Y. Endoh, S. Wakimoto, K. Yamada, R. W. Erwin, S.-H. Lee, and G. Shirane, Neutron-scattering study of spin-density wave order in the superconducting state of excess-oxygen-doped La_2CuO_{4+y}, Phys. Rev. B **60**, 3643 (1999).

[16] A. R. Moodenbaugh, Y. Xu, M. Suenaga, T. J. Folkerts, and R. N. Shelton, Superconducting properties of $La_{2-x}Ba_xCuO_4$, Phys. Rev. B **38**, 4596 (1988).

[17] J. M. Tranquada, G. D. Gu, M. Hücker, Q. Jie, H.-J. Kang, R. Klingeler, Q. Li, N. Tristan, J. S. Wen, G. Y. Xu, Z. J. Xu, J. Zhou, and M. v. Zimmermann, Evidence for unusual superconducting correlations coexisting with stripe order in $La_{1.875}Ba_{0.125}CuO_4$, Phys. Rev. B **78**, 174529 (2008).

[18] M. Hücker, M. v. Zimmermann, G. D. Gu, Z. J. Xu, J. S. Wen, G. Xu, H. J. Kang, A. Zheludev, and J. M. Tranquada, Stripe order in superconducting $La_{2-x}Ba_xCuO_4$ ($0.095 \leqslant x \leqslant 0.155$), Phys. Rev. B **83**, 104506 (2011).

[19] J. Chang, Ch. Niedermayer, R. Gilardi, N. B. Christensen, H. M. Rønnow, D. F. McMorrow, M. Ay, J. Stahn, O. Sobolev, A. Hiess, S. Pailhes, C. Baines, N. Momono, M. Oda, M. Ido, and J. Mesot, Tuning competing orders in $La_{2-x}Sr_xCuO_4$ cuprate superconductors by the application of an external magnetic field, Phys. Rev. B **78**, 104525 (2008).

[20] B. Lake, H. M. Rønnow, N. B. Christensen, G. Aeppli, K. Lefmann, D. F. McMorrow, P. Vorderwisch, P. Smeibidl, N. Mangkorntong, T. Sasagawa, M. Nohara, H. Takagi, and T. E. Mason, Antiferromagnetic order induced by an applied magnetic field in a high-temperature superconductor, Nature (London) **415**, 299 (2002).

[21] A. T. Rømer, J. Chang, N. B. Christensen, B. M. Andersen, K. Lefmann, L. Mähler, J. Gavilano, R. Gilardi, Ch Niedermayer, H. M. Rønnow, A. Schneidewind, P. Link, M. Oda, M. Ido, N. Momono, and J. Mesot, Glassy low-energy spin fluctuations and anisotropy gap in $La_{0.88}Sr_{0.12}CuO_4$, Phys. Rev. B **87**, 144513 (2013).

[22] B. Khaykovich, S. Wakimoto, R. J. Birgeneau, M. A. Kastner, Y. S. Lee, P. Smeibidl, P. Vorderwisch, and K. Yamada, Field-induced transition between magnetically disordered and ordered phases in underdoped $La_{2-x}Sr_xCuO_4$, Phys. Rev. B **71**, 220508(R) (2005).

[23] J. Chang, N. B. Christensen, Ch Niedermayer, K. Lefmann, H. M. Rønnow, D. F. McMorrow, A. Schneidewind, P. Link, A. Hiess, M. Boehm, R. Mottl, S. Pailhés, N. Momono, M. Oda, M. Ido, and J. Mesot, Magnetic-field-induced soft-mode quantum phase transition in the high-temperature superconductor $La_{1.855}Sr_{0.145}CuO_4$: An inelastic neutron-scattering study, Phys. Rev. Lett. **102**, 177006 (2009).

[24] M. Frachet, I. Vinograd, R. Zhou, S. Benhabib, S. Wu, H. Mayaffre, S. Krämer, S. K. Ramakrishna, A. P. Reyes, J. Debray, T. Kurosawa, N. Momono, M. Oda, S. Komiya, S. Ono, M. Horio, J. Chang, C. Proust, D. LeBoeuf, and M. H. Julien, Hidden magnetism at the pseudogap critical point of a cuprate superconductor, Nat. Phys. **16**, 1064 (2020).

[25] B. Khaykovich, Y. S. Lee, R. W. Erwin, S.-H. Lee, S. Wakimoto, K. J. Thomas, M. A. Kastner, and R. J. Birgeneau, Enhancement of long-range magnetic order by magnetic field in superconducting La_2CuO_{4+y}, Phys. Rev. B **66**, 014528 (2002).

[26] A. T. Savici, Y. Fudamoto, I. M. Gat, T. Ito *et al.*, Muon spin relaxation studies of incommensurate magnetism and superconductivity in stage-4 $La_2CuO_{4.11}$ and $La_{1.88}Sr_{0.12}CuO_4$, Phys. Rev. B **66**, 014524 (2002).

[27] M. Kofu, S.-H. Lee, M. Fujita, H.-J. Kang, H. Eisaki, and K. Yamada, Hidden quantum spin-gap state in the static stripe phase of high-temperature $La_{2-x}Sr_xCuO_4$ superconductors, Phys. Rev. Lett. **102**, 047001 (2009).

[28] S. A. Kivelson, G. Aeppli, and V. J. Emery, Thermodynamics of the interplay between magnetism and high-temperature superconductivity, Proc. Natl. Acad. Sci. USA **98**, 11903 (2001).

[29] H. E. Mohottala, B. O. Wells, J. I. Budnick, Wi. a. Hines, Chr. Niedermayer, L. Udby, C. Bernhard, A. R. Moodenbaugh, and F.-Ch. Chou, Phase separation in superoxygenated $La_{2-x}Sr_xCuO_{4-y}$, Nat. Mater. **5**, 377 (2006).

[30] L. Udby, J. Larsen, N. B. Christensen, M. Boehm, Ch. Niedermayer, H. E. Mohottala, T. B. S. Jensen, R. Toft-Petersen, F. C. Chou, N. H. Andersen, K. Lefmann, and B. O. Wells, Measurement of unique magnetic and superconducting phases in oxygen-doped high-temperature superconductors $La_{2-x}Sr_xCuO_{4+y}$, Phys. Rev. Lett. **111**, 227001 (2013).

[31] H. Jacobsen, S. L. Holm, M.-E. Lăcătuşu, A. T. Rømer, M. Bertelsen, M. Boehm, R. Toft-Petersen, J.-C. Grivel, S. B. Emery, L. Udby, B. O. Wells, and K. Lefmann, Distinct nature of static and dynamic magnetic stripes in cuprate superconductors, Phys. Rev. Lett. **120**, 037003 (2018).

[32] S. Wakimoto, R. J. Birgeneau, Y. S. Lee, and G. Shirane, Hole concentration dependence of the magnetic moment in superconducting and insulating $La_{2-x}Sr_xCuO_4$, Phys. Rev. B **63**, 172501 (2001).

[33] Q. Li, M. Hücker, G. D. Gu, A. M. Tsvelik, and J. M. Tranquada, Two-dimensional superconducting fluctuations in stripe-ordered $La_{1.875}Ba_{0.125}CuO_4$, Phys. Rev. Lett. **99**, 067001 (2007).

[34] S. Tajima, T. Noda, H. Eisaki, and S. Uchida, *c*-axis optical response in the static stripe ordered phase of the cuprates, Phys. Rev. Lett. **86**, 500 (2001).

[35] A. A. Schafgans, A. D. LaForge, S. V. Dordevic, M. M. Qazilbash, W. J. Padilla, K. S. Burch, Z. Q. Li, S. Komiya, Y. Ando, and D. N. Basov, Towards a two-dimensional superconducting state of $La_{2-x}Sr_xCuO_4$ in a moderate external magnetic field, Phys. Rev. Lett. **104**, 157002 (2010).

[36] A. A. Schafgans, C. C. Homes, G. D. Gu, S. Komiya, Y. Ando, and D. N. Basov, Breakdown of the universal Josephson relation in spin-ordered cuprate superconductors, Phys. Rev. B **82**, 100505(R) (2010).

[37] A. Himeda, T. Kato, and M. Ogata, Stripe states with spatially oscillating *d*-wave superconductivity in the two-dimensional $t - t' - J$ model, Phys. Rev. Lett. **88**, 117001 (2002).

[38] E. Berg, E. Fradkin, E.-A. Kim, S. A. Kivelson, V. Oganesyan, J. M. Tranquada, and S. C. Zhang, Dynamical layer decoupling in a stripe-ordered high-T_c superconductor, Phys. Rev. Lett. **99**, 127003 (2007).

[39] D. F. Agterberg, J. C. Séamus Davis, S. D. Edkins, E. Fradkin, D. J. Van Harlingen, S. A. Kivelson, P. A. Lee, L. Radzihovsky, J. M. Tranquada, and Y. Wang, The physics of pair-density waves: Cuprate superconductors and beyond, Annu. Rev. Condens. Matter Phys. **11**, 231 (2020).

[40] E. Fradkin, S. A. Kivelson, and J. M. Tranquada, Colloquium: Theory of intertwined orders in high temperature superconductors, Rev. Mod. Phys. **87**, 457 (2015).

[41] B. Lorenz, Z. G. Li, T. Honma, and P. H. Hor, An intrinsic tendency of electronic phase separation into two superconducting states in $La_{2-x}Sr_xCuO_{4+y}$, Phys. Rev. B **65**, 144522 (2002).

[42] C. R. H. Bahl, P. Andersen, S. N. Klausen, and K. Lefmann, The monochromatic imaging mode of a RITA-type neutron spectrometer, Nucl. Instrum. Methods Phys. Res. Sect. B **226**, 667 (2004).

[43] C. R. H. Bahl, K. Lefmann, A. B. Abrahamsen, H. M. Rønnow, F. Saxild, T. B. S. Jensen, L. Udby, N. H. Andersen, N. B. Christensen, H. S. Jakobsen, T. Larsen, P. S. Häfliger, S. Streule, and Ch. Niedermayer, Inelastic neutron scattering experiments with the monochromatic imaging mode of the RITA-II spectrometer, Nucl. Instrum. Methods Phys. Res. Sect. B **246**, 452 (2006).

[44] M. Boehm, A. Hiess, J. Kulda, S. Roux, and J. Saroun, ThALES - three axis low energy spectroscopy at the Institut Laue-Langevin, Meas. Sci. Technol. **19**, 034024 (2008).

[45] H. Jacobsen, M. Boehm, S. Holm-Dahlin, K. Lefmann, Ch. Niedermayer, A. Piovano, T. B. Tejsner, A. E. Tutueanu, L. Udby, and B. Wells, Institut Laue-Langevin (ILL), https://doi.ill.fr/10.5291/ILL-DATA.4-02-479 (2016).

[46] K. Lefmann, M. Boehm, S. Holm-Dahlin, H. Jacobsen, M.-E. Lacatusu, and L. Udby, Institut Laue-Langevin (ILL), https://doi.ill.fr/10.5291/ILL-DATA.TEST-2473 (2016).

[47] K. Yamada, C. H. Lee, K. Kurahashi, J. Wada, S. Wakimoto, S. Ueki, H. Kimura, Y. Endoh, S. Hosoya, G. Shirane, R. J. Birgeneau, M. Greven, M. A. Kastner, and Y. J. Kim, Doping dependence of the spatially modulated dynamical spin correlations and the superconducting transition temperature in $La_{2-x}Sr_xCuO_4$, Phys. Rev. B **57**, 6165 (1998).

[48] A. Amato, H. Luetkens, K. Sedlak, A. Stoykov, R. Scheuermann, M. Elender, A. Raselli, and D. Graf, The new versatile general purpose surface-muon instrument (GPS) based on silicon photomultipliers for μSR measurements on a continuous-wave beam, Rev. Sci. Instrum. **88**, 093301 (2017).

[49] R. Scheuermann, Paul Scherrer Institut (PSI), https://www.psi.ch/en/smus/hal-9500 (2020).

[50] G. Shirane, S. M. Shapiro, and J. M. Tranquada, *Neutron Scattering with a Triple-Axis Spectrometer* (Cambridge University Press, Cambridge, 2002).

[51] P. Kjaer Willendrup and K. Lefmann, Mcstas (i): Introduction, use, and basic principles for ray-tracing simulations, J. Neutron Res. **22**, 1 (2020).

[52] L. Udby, P. K. Willendrup, E. Knudsen, Ch. Niedermayer, U. Filges, N. B. Christensen, E. Farhi, B. O. Wells, and K. Lefmann, Analysing neutron scattering data using McStas virtual experiments, Nucl. Instrum. Methods Phys. Res. Sect. A **634**, S138 (2011).

[53] S. J. Blundell, Spin-polarized muons in condensed matter physics, Contemp. Phys. **40**, 175 (1999).

[54] Y. Wang and H.-H. Wen, Doping dependence of the upper critical field in $La_{2-x}Sr_xCuO_4$ from specific heat, Europhys. Lett. **81**, 57007 (2008).

[55] N. B. Christensen, J. Chang, J. Larsen, M. Fujita, M. Oda, M. Ido, N. Momono, E. M. Forgan, A. T. Holmes, J. Mesot, M. Huecker, and M. v. Zimmermann, Bulk charge stripe order competing with superconductivity in $La_{2-x}Sr_xCuO_4$ ($x = 0.12$), arXiv:1404.3192.

[56] T. P. Croft, C. Lester, M. S. Senn, A. Bombardi, and S. M. Hayden, Charge density wave fluctuations in $La_{2-x}Sr_xCuO_4$ and their competition with superconductivity, Phys. Rev. B **89**, 224513 (2014).

[57] Z. Zhang, R. Sutarto, F. He, F. C. Chou, L. Udby, S. L. Holm, Z. H. Zhu, W. A. Hines, J. I. Budnick, and B. O. Wells, Nematicity and charge order in superoxygenated $La_{2-x}Sr_xCuO_{4+y}$, Phys. Rev. Lett. **121**, 067602 (2018).

[58] S. Wakimoto, G. Shirane, Y. Endoh, K. Hirota, S. Ueki, K. Yamada, R. J. Birgeneau, M. A. Kastner, Y. S. Lee, P. M. Gehring, and S. H. Lee, Observation of incommensurate magnetic correlations at the lower critical concentration for superconductivity in $La_{2-x}Sr_xCuO_4$, Phys. Rev. B **60**, R769 (1999).

[59] H. Jacobsen, I. A. Zaliznyak, A. T. Savici, B. L. Winn, S. Chang, M. Hucker, G. D. Gu, and J. M. Tranquada, Neutron scattering study of spin ordering and stripe pinning in superconducting $La_{1.93}Sr_{0.07}CuO_4$, Phys. Rev. B **92**, 174525 (2015).

[60] A. T. Rømer, P. J. Ray, H. Jacobsen, L. Udby, B. M. Andersen, M. Bertelsen, S. L. Holm, N. B. Christensen, R. Toft-Petersen, M. Skoulatos, M. Laver, A. Schneidewind, P. Link, M. Oda, M. Ido, N. Momono, and K. Lefmann, Field-induced interplanar magnetic correlations in the high-temperature superconductor $La_{1.88}Sr_{0.12}CuO_4$, Phys. Rev. B **91**, 174507 (2015).

[61] D. Haug, V. Hinkov, A. Suchaneck, D. S. Inosov, N. B. Christensen, Ch. Niedermayer, P. Bourges, Y. Sidis, J. T. Park, A. Ivanov, C. T. Lin, J. Mesot, and B. Keimer, Magnetic-field-enhanced incommensurate magnetic order in the underdoped high-temperature superconductor $YBa_2Cu_3O_{6.45}$, Phys. Rev. Lett. **103**, 017001 (2009).

[62] J. S. Wen, Z. J. Xu, G. Y. Xu, J. M. Tranquada, G. Gu, S. Chang, and H. J. Kang, Magnetic field induced enhancement of spin-order peak in $La_{1.875}Ba_{0.125}CuO_4$, Phys. Rev. B **78**, 212506 (2008).

[63] B. Lake, N. B. Christensen K. Lefmann, G. Aeppli, D. F. McMorrow, H. M. Ronnow, P. Vorderwisch, P. Smeibidl, N. Mangkorntong, T. Sasagawa, M. Nohara, and H. Takagi, Three-dimensionality of field-induced magnetism in a high-temperature superconductor, Nat. Mater. **4**, 658 (2005).

[64] L. Udby, N. H. Andersen, F. C. Chou, N. B. Christensen, S. B. Emery, K. Lefmann, J. W. Lynn, H. E. Mohottala, Ch. Niedermayer, and B. O. Wells, Magnetic ordering in electronically phase-separated $(La_{1-x}Sr_x)_2CuO_{4+y}$: Neutron diffraction experiments, Phys. Rev. B **80**, 014505 (2009).

[65] M. Fujita, K. Yamada, H. Hiraka, P. M. Gehring, S. H. Lee, S. Wakimoto, and G. Shirane, Static magnetic correlations near the insulating-superconducting phase boundary in $La_{2-x}Sr_xCuO_4$, Phys. Rev. B **65**, 064505 (2002).

[66] D. G. Hawthorn, R. W. Hill, C. Proust, F. Ronning, M. Sutherland, E. Boaknin, C. Lupien, M. A. Tanatar, J. Paglione, S. Wakimoto, H. Zhang, L. Taillefer, T. Kimura, M. Nohara, H. Takagi, and N. E. Hussey, Field-induced thermal metal-to-insulator transition in underdoped $La_{2-x}Sr_xCuO_4$, Phys. Rev. Lett. **90**, 197004 (2003).

[67] P. J. Ray, N. H. Andersen, T. B. S. Jensen, H. E. Mohottala, Ch. Niedermayer, K. Lefmann, B. O. Wells, M. v. Zimmermann, and L. Udby, Staging superstructures in high-T_c Sr/O codoped $La_{2-x}Sr_xCuO_{4+y}$, Phys. Rev. B **96**, 174106 (2017).

[68] E. S. Bozin, R. Zhong, K. R. Knox, G. Gu, J. P. Hill, J. M. Tranquada, and S. J. L. Billinge, Reconciliation of local and long-range tilt correlations in underdoped $La_{2-x}Ba_xCuO_4$ ($0 \leqslant x \leqslant 0.155$), Phys. Rev. B **91**, 054521 (2015).

[69] M. Tinkham, *Introduction to Superconductivity* (McGraw-Hill, New York, 1975).

[70] P. J. M. van Bentum, H. van Kempen, L. E. C. van de Leemput, J. A. A. J. Perenboom, L. W. M. Schreurs, and P. A. A. Teunissen, High-field measurements on the high-T_c superconductors $La_{1.85}Sr_{0.15}CuO_{4-\delta}$ and $YBa_2Cu_3O_{7-\delta}$, Phys. Rev. B **36**, 5279 (1987).

[71] W. K. Kwok, G. W. Crabtree, D. G. Hinks, D. W. Capone, J. D. Jorgensen, and K. Zhang, Normal- and superconducting-state properties of $La_{1.85}Sr_{0.15}CuO_4$, Phys. Rev. B **35**, 5343 (1987).

[72] N. R. Werthamer, E. Helfand, and P. C. Hohenberg, Temperature and purity dependence of the superconducting critical field, H_{c2}. III. Electron spin and spin-orbit effects, Phys. Rev. **147**, 295 (1966).

[73] D. Nakamura, T. Adachi, K. Omori, Y. Koike, and S. Takeyama, Pauli-limit upper critical field of high-temperature superconductor $La_{1.84}Sr_{0.16}CuO_4$, Sci. Rep. **9**, 16949 (2019).

[74] C. Kittel, *Introduction to Solid State Physics*, 8th ed. (John Wiley and Sons, Inc, University of California, Berkeley, 2004).

[75] C. Boyd and P. W. Phillips, Single-parameter scaling in the magnetoresistance of optimally doped $La_{2-x}Sr_xCuO_4$, Phys. Rev. B **100**, 155139 (2019).

[76] R. S. Hayano, Y. J. Uemura, J. Imazato, N. Nishida, T. Yamazaki, and R. Kubo, Zero- and low-field spin relaxation studied by positive muons, Phys. Rev. B **20**, 850 (1979).

[77] B. O. Wells, R. J. Birgeneau, F. C. Chou, Y. Endoh, D. C. Johnston, M. A. Kastner, Y. S. Lee, G. Shirane, J. M. Tranquada, and K. Yamada, Intercalation and staging behavior in super-oxygenated $La_2CuO_{4+\delta}$, Z. Phys. B **100**, 535 (1996).